Steric Effects in the Scattering of Oriented CH_3Cl Molecular Beam from a Graphite Surface: Weak Interaction of Physisorption†

Tetsuya Fukuyama,‡ Michio Okada,*,‡,§,∥ and Toshio Kasai*,‡

Department of Chemistry, Graduate School of Science, Osaka University, 1-1 Machikaneyama-cho, Toyonaka, Osaka 560-0043, Japan, Renovation Center of Instruments for Science Education and Technology, Osaka University, 1-2 Machikaneyama-cho, Toyonaka, Osaka 560-0043, Japan, and PRESTO, Japan Science and Technology Agency, 4-1-18 Honcho, Kawaguchi, Saitama 332-0012, Japan

Received: May 26, 2009; Revised Manuscript Received: June 28, 2009

We report results of a study on steric effects appearing in the scattering of an oriented CH_3Cl molecular beam from highly oriented pyrolytic graphite (HOPG) surface at 300 K. Data presented here show that the scattered CH_3Cl beam intensity measured at a fixed scattering angle clearly depends on the initial molecular orientation toward the HOPG surface. The scattered CH_3Cl beam intensity for the CH_3-end collision is larger than that for the Cl-end collision, suggesting that strong anisotropy of the interaction potential induces the molecular-orientation-dependent energy dissipation during transient trapping into the physisorption well.

1. Introduction

It is expected that the molecular orientation of an incoming molecule on a surface may be quite important in dynamical processes in chemical reactions.[1−41] In particular, the steric effect on the interaction of polyatomic molecules from surfaces is one of the central topics in the fields of organic chemistry, catalytic chemistry, biochemistry, and so on. Although there are a lot of studies on the steric effects of diatomic molecules on surfaces,[2−16,26−31,35−37,41] the works on polyatomic molecules are rare.[1,17−25,31−33,38−40] The steric effects of a polyatomic system was first reported by Novakoshi and McClelland in the CF_3H scattering from Ag(111) surface.[1] They determined the molecular orientation of the outgoing molecule after collisions. Bernstein and coworkers reported a series of systematic investigations of steric effects in the scattering of polyatomic halides from highly oriented pyrolytic graphite (HOPG).[17−25] Both systems of Ag(111) and HOPG provide weakly bound physisorption.

Very recently, we reported the steric effects in the dissociative adsorption of polyatomic CH_3Cl on Si(100) and proposed that the transient trapping into the weakly bound precursor state contributes to the observed molecular orientation effects.[38−40] Therefore, to clarify the importance of the dynamical process in such transient trapping into a precursor state, the weakly bound CH_3Cl/HOPG is one of the best candidates.

In the present article, we report the steric effects in the scattering of CH_3Cl from a HOPG surface at 300 K. We measured the molecular orientation effects under better experimental conditions using shorter pulse of beam and effective differential pumping of the detector, as compared with those in the previous work reported by Bernstein and coworkers.[18,20] These improvements in the experimental conditions enable us to separate the scattered beam profile into two components explicitly (vide infra). In all possible scattering geometry in our apparatus, the scattered CH_3Cl beam intensity in the CH_3-end approach is found to be higher than that in the Cl-end approach. This result suggests that the trapping probability for the Cl-end approach is higher than that for the CH_3-end approach.

2. Experimental Section

A schematic view of the ultrahigh vacuum (UHV)-compatible oriented molecular beam apparatus adapted for gas-surface scattering experiments is shown in Figure 1.[42] The details of the apparatus are already described elsewhere.[42] In brief, the apparatus consists of an oriented molecular beamline connected to a scattering chamber with typical base pressure of 1×10^{-10} Torr. The 10 Hz and 200 μs fwhm (full width at a half-maximum) pulsed CH_3Cl molecular beam is generated by the expansion of CH_3Cl (5%) seeded in He with a pulsed valve. The rotational-state-selected CH_3Cl beam was focused on the surface, employing a 1 m long hexapole state selector. The orientation of CH_3Cl can be controlled by changing the polarity of the rod voltage installed in front of the surface.

The incident beam profile was determined from the time-of-flight (TOF) measurements using a differentially pumped quadrupole mass spectrometer (QMS). In the surface scattering experiments requiring the high beam intensity, we use the pulse nozzle to generate the pulsed beam (without a beam chopper wheel producing shorter well-defined pulses) and thus determine the beam profile from the pulse-nozzle-generated beam itself. In typical, the estimated stream velocity of incident CH_3Cl was 1100 m s^{-1} (320 meV) and the velocity width was 95 m s^{-1}. In the measurement of the intense incident beam profile, the present differentially pumping system was not so effective that the beam profile determination is accompanied with some ambiguity because of the beam-induced background pressure rise in the detection chamber. However, the obtained beam profile is sufficient enough for the present scattering experiments.[43]

Figure 2 shows the focusing curve of CH_3Cl (5%) seeded in He, obtained by measuring the TOF profile of the CH_3Cl beam as a function of the hexapole voltage ($\pm V_0$). For these measurements, we move the differentially pumped QMS (Figure 1) on the line in sight of the molecular beam. At $V_0 = 0$, the

† Part of the "Vincenzo Aquilanti Festschrift".

* Corresponding authors. (M.O.) okada@chem.sci.osaka-u.ac.jp. (T.K.) tkasai@chem.sci.osaka-u.ac.jp.

‡ Department of Chemistry, Graduate School of Science, Osaka University.

§ Renovation Center of Instruments for Science Education and Technology, Osaka University.

∥ PRESTO.

10.1021/jp904893z
Published on Web 07/14/2009

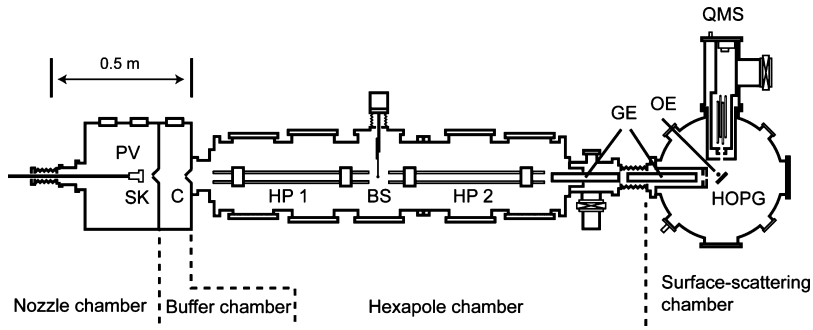

Figure 1. Schematic top view of oriented molecular beamline and surface reaction analysis chamber: PV, pulsed valve; SK, skimmer; C, beam collimator; HP1, HP2, hexapole device; BS, beam stop; GE, guiding electrode; OE, orientation electrode; QMS, quadrupole mass spectrometer.

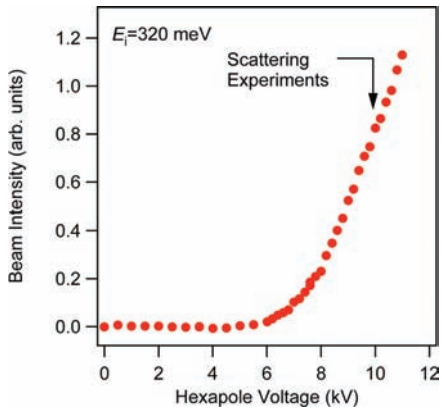

Figure 2. Focusing curves for 320 meV CH_3Cl (5%) seeded in He. The hexapole voltage where the surface-scattering experiments were performed is indicated by the arrow.

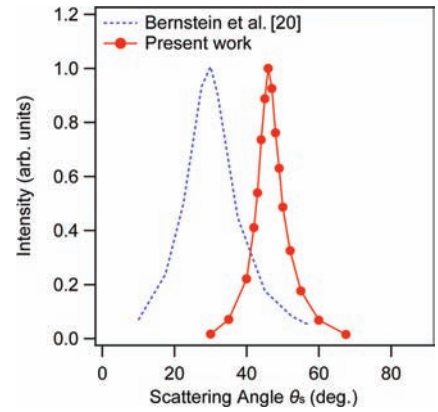

Figure 3. Angular distribution of the scattered He atoms in the pure He incidence on the HOPG surface at 300 K. The total scattering angle of $(\theta_i + \theta_s)$ was 90°. The data measured at $\theta_i + \theta_s = 60°$ by Bernstein and coworkers[20] are also indicated by the blue dotted line.

CH_3Cl beam with only diverging trajectories was perfectly shadowed by the beam stop (7 mm in diameter) and cannot enter the surface-scattering chamber. As a result of simulation, at $V_0 = \pm 10$ kV, where the surface scattering experiments were performed, $|JKM\rangle = |111\rangle$ is dominant (more than 80%) and the expected first Legendre moment $\langle \cos \gamma \rangle$ of the molecular orientation distribution was 0.50.

The CH_3Cl molecules scattered from the HOPG surface were measured at a fixed angle of $\theta_i + \theta_s = 90°$ between the incident beam and the detector, as shown in Figure 1. Here $\theta_i(\theta_s)$ is the angle enclosed by the surface normal and incoming (scattered) beam and was varied by rotating the sample. The acceptance angle of the detector was 2.9°. The orientation of the CH_3Cl molecule was controlled with the voltage applied to an orientation electrode at 20 mm in front of the HOPG surface. In the steric effect measurements, the polarity of the voltage applied to the orientation electrode was switched every 100 s (every 1000 pulsed beams) between +700 and −700 V. The obtained orientation-field strength of 350 V cm^{-1} is enough to obtain almost perfect orientation for CH_3Cl.[44]

The HOPG (NT-MDT, size: 12 × 12 × 1.5 mm) was cleaved by the cellophane tape in the air and mounted on the sample holder made of molybdenum. The HOPG sample was heated at ~700 K during a 24 h bakeout of the UHV chamber and finally heated to 700 K for 30 min under the UHV condition. We performed the He atom scattering to check the surface cleanliness and flatness. Figure 3 shows the angular distribution of scattered He from the HOPG surface at 300 K after the sample preparation. The scattering intensity in the specular scattering angle, $\theta_s = 45°$, reached the maximum, suggesting that the alignment of the scattering geometry is exact enough. Furthermore, the angular fwhm width of scattered He intensity was about 7.5° and was narrower than that of the previous work,[20] as shown in Figure 3. Therefore, the clean and flat-terrace HOPG surface was obtained after our preparation, and the performance of this apparatus was enough for the present purpose of the scattering experiments. During the surface-scattering experiment requiring a long data acquisition time of ~24 h, the surface was clean enough that no CH_3Cl molecules were adsorbed on the HOPG surface at 300 K, and no changes were detected in the He scattering profile during the measurements.

3. Results and Discussions

Figure 4 shows the typical TOF spectrum of CH_3Cl scattered at $\theta_s = 56°$ from the HOPG surface at 300 K in the focused but randomly oriented CH_3Cl beam incidence at 320 meV and $\theta_i = 34°$. We analyze the TOF spectrum on the basis of the two-component model[45,46] where the scattering processes can be separated into a direct-inelastic scattering without surface residence and a trapping desorption with surface residence as $F(t) = F_{direct}(t) + F_{trap}(t)$, where $F(t)$, $F_{direct}(t)$, and $F_{trap}(t)$ are the scattered beam density profile, the direct-inelastic, and the trapping desorption components of the profile, respectively. $F_{trap}(t)$ corresponds to the Maxwellian velocity distribution with a finite residence time (≤300 μs[47]) at the surface temperature (T_s) of 300 K.

According to Sasaki and Yoshida,[45,46] $F_{trap}(t)$ becomes the convolution of the surface residence (time constant τ), the velocity distribution of incident CH_3Cl ($f^i_{dM}(t)$), and that of desorbed CH_3Cl ($f^s_{trap}(t)$). Therefore, $F_{trap}(t)$ can be can be expressed as

$$F_{\text{trap}}(t) = A\int_0^t dt_2 f^{\text{s}}_{\text{trap}}(t-t_2)(t-t_2)\times \int_0^{t_2} dt_1 \exp\left(-\frac{t_2-t_1}{\tau}\right) f^{\text{i}}_{\text{dM}}(t_1) \quad (1)$$

Here $f^{\text{i}}_{\text{dM}}(t) = at^{-5}\exp[-((L/t-v_s)/\sigma)^2]$, where L is the length of the flight path for the incident beam, v_s is a stream velocity, σ is a velocity spread, and A and a are constant factors. Because thermal equilibrium must be realized during a long surface residence, $f^{\text{s}}_{\text{trap}}(t)$ is considered to be Maxwellian for surface temperature (T_s). Here $f^{\text{s}}_{\text{trap}}(t)$ can be expressed as

$$f^{\text{s}}_{\text{trap}}(t) = a' t^{-5}\exp\left[-\left(\frac{L_s/t}{\beta}\right)^2\right], \quad (\beta = \sqrt{2kT_s/m}) \quad (2)$$

where L_s is the distance from the sample to the QMS, k is Boltzmann constant, m is molecular mass, and a' is a constant.

The component without a surface residence, $F_{\text{direct}}(t)$, also becomes the convolution[45,46]

$$F_{\text{direct}}(t) = B\int_0^t dt_1 f^{\text{s}}_{\text{direct}}(t-t_1)(t-t_1) f^{\text{i}}_{\text{dM}}(t_1) \quad (3)$$

where $f^{\text{s}}_{\text{direct}}(t)$ represents the scattered CH_3Cl velocity distributions in the direct-inelastic component. We assume that the scattered CH_3Cl has a translationally drifting Maxwellian velocity distribution because it is possible that thermal equilibrium is not realized during scattering in this component. Therefore, $f^{\text{s}}_{\text{direct}}$ is given by

$$f^{\text{s}}_{\text{direct}}(t) = bt^{-5}\exp\left[-\left(\frac{L_s/t - s}{\alpha}\right)^2\right] \quad (4)$$

where s is a stream velocity, α is a velocity spread, and b is a constant factor.

The measured TOF spectrum can be reproduced satisfactorily with this model. The expected TOF spectrum assumed for the elastically scattered CH_3Cl is also added for comparison in Figure 4. It clearly demonstrates that the CH_3Cl molecule suffers a significant energy loss, even in the direct-inelastic scattering process. According to the fitting parameters reproducing the TOF spectrum, the kinetic energy of the CH_3Cl molecule in the direct-inelastic scattering is 18 meV. Therefore, 94% in the initial translational energy of 320 meV is dissipated.

Figure 5a shows the scattering angle (θ_s) dependence of the TOF spectra for CH_3Cl scattered from the HOPG surface at 300 K in the 320 meV randomly oriented CH_3Cl incidence. In our measurements, $\theta_i + \theta_s$ was fixed at 90°. It is found that the two-component model of $F_{\text{direct}}(t)$ and $F_{\text{trap}}(t)$ can reproduce well the TOF spectra for all scattering angles with the same fitting parameters, except for the intensities and the small changes in the final kinetic energy for the direct-inelastic scattering. The TOF spectra at $\theta_s \leq 45°$ mainly consist of the trapping desorption component. However, the TOF spectra at $\theta_s \approx 56°$ mainly consist of the direct-inelastic scattering component. Figure 5b summarizes the θ_s dependence of the integrated intensity of the two components of $F_{\text{direct}}(t)$ and $F_{\text{trap}}(t)$. The distribution of the direct-inelastic component (filled squares) is sharp and, therefore, directional, which is consistent with the scattering process. However, the trapping desorption component displays the broad θ_s distribution. We approximate it with the cosine distribution, as indicated in Figure 5b. We varied θ_s by rotating the HOPG sample. Therefore, the cosine distribution is expected for the trapping desorption unless the surface trapping probability depends on the surface-normal component of the kinetic energy. In Figure 5b, the cosine distribution can almost reproduce the data, except for $\theta_s \leq 40°$ corresponding to the glancing incidence with smaller surface-normal energy.

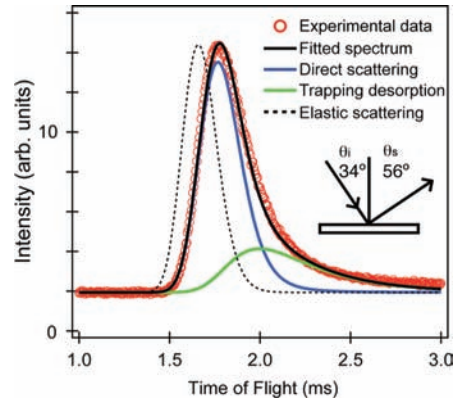

Figure 4. TOF spectrum (red circles) for CH_3Cl scattered $\theta_s = 56°$ from HOPG at 300 K in the 320 meV randomly oriented CH_3Cl incidence at $\theta_i = 34°$. The fitted line (black solid line) is based on the two-component model of the direct-inelastic scattering (blue solid line) and the trapping desorption (green solid line). The dotted line corresponds to the expected TOF spectrum assumed for the elastically scattered CH_3Cl.

The average kinetic energy of the direct-inelastic scattering is ~18 meV, which does not depend strongly on the scattering angle, θ_s. Therefore, the average 94% of the initial translational energy (320 meV) is dissipated during the scattering process. Such a large energy loss cannot be explained with the simple hard cube (HC) model, where the surface-parallel component of the momentum is conserved during the scattering process on the surface. Moreover, the ratio of the energy loss relative to the incident energy is much larger than that in other systems such as Xe from HOPG[48,49] and Ne and CH_4 from graphitic monolayer on Pt.[50] Bernstein and coworkers employed the modified HC model, including the parallel-momentum loss due to the rotational excitation, to the *t*-butyl chloride scattering from HOPG.[23] However, it required the unphysical parameters to reproduce their data. The main difference between the particles (Ne, Xe, and CH_4) and CH_3Cl is a large permanent dipole moment of CH_3Cl (6.24×10^{-30} C m[51]) and thus its polarizability. The permanent dipole in front of the HOPG surface induces its mirror image charges in the classical electromagnetic sense.[24] As a result, the interaction becomes further attractive and thus induces further energy dissipation into the surface phonons, electron−hole pairs, and rotational excitations of CH_3Cl. The parallel-momentum conservation will not hold in such a case. Therefore, it is rather surprising that the molecule suffering such large energy losses (in scrambling) still shows the direct-scattering character in the angular distribution. Clarifying the energy-loss processes during such a scattering will be one of our continued studies.

Figure 6 shows the molecular-orientation dependence of the TOF spectra for the oriented 320 meV CH_3Cl incidence at $\theta_i = 34°$ (the detection at $\theta_s = 56°$) on the HOPG surface at 300 K. Clearly, the scattering intensity for the CH_3-end collision is higher than that for the Cl-end collision. This result is consistent with the experimental results obtained by Bernstein and coworkers,[18,20] although we improve the experimental conditions much better than theirs, that is, shorter pulsed molecular beam, effective differential pumping of the detector, and the

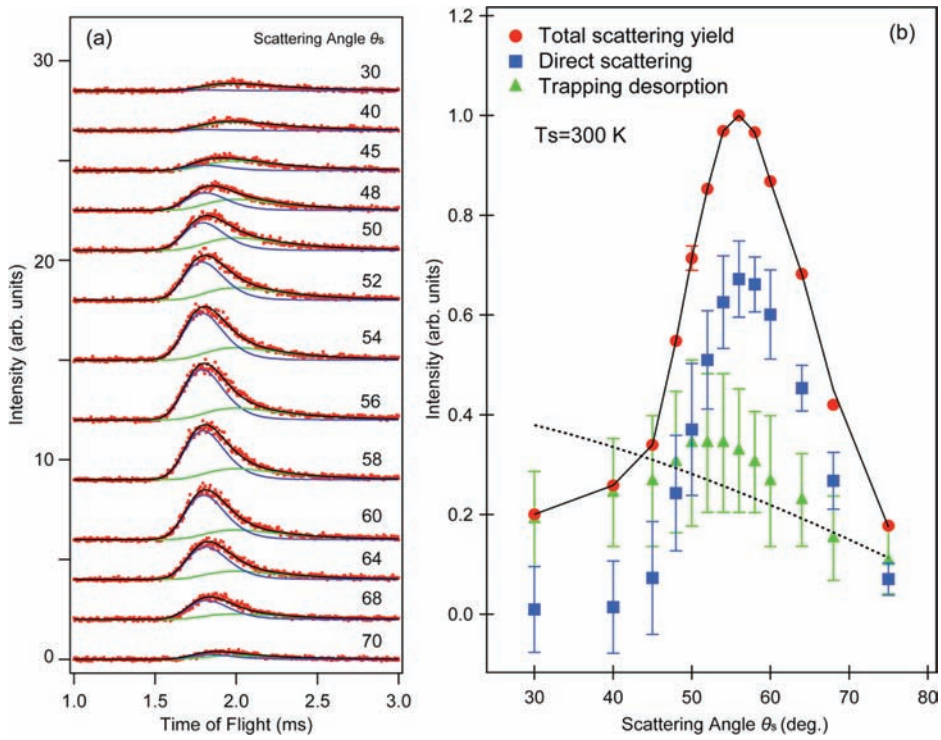

Figure 5. (a) θ_s dependence of the TOF spectra for CH_3Cl scattered from HOPG at 300 K in the 320 meV randomly oriented CH_3Cl incidence. The fitted line (black solid line) is based on the two-component model of the direct-inelastic scattering (blue solid line) and the trapping desorption (green solid line). (b) θ_s dependence of the integrated intensity of the TOF spectra in part a; total intensity (red circles) and the components of the direct-inelastic scattering (blue squares) and the trapping desorption (green triangles). Dashed line indicates the cosine distribution fitting the trapping desorption.

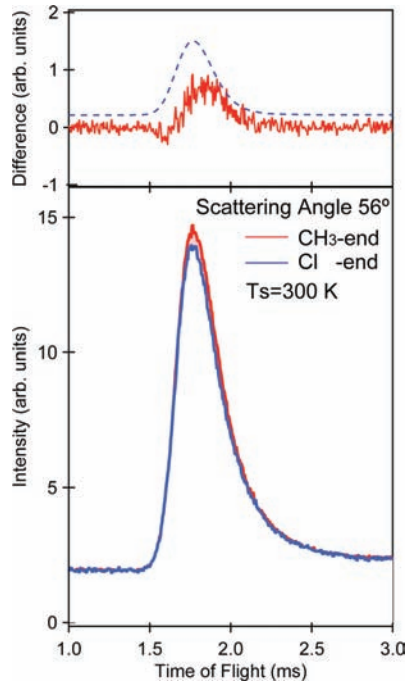

Figure 6. (Bottom panel) Molecular-orientation dependence of the TOF spectra at $\theta_s = 56°$ for the CH_3-end (red line) and the Cl-end (blue line) approaches in the 320 meV CH_3Cl incidence at $\theta_i = 34°$. (Top panel) The difference (red line) of the TOF spectra in the bottom panel. The dashed blue line corresponds to the direct-inelastic scattering in Figure 4.

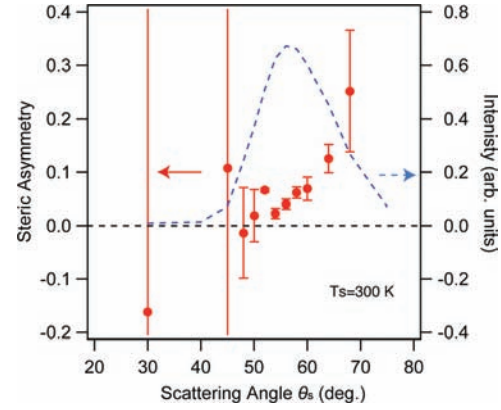

Figure 7. θ_s dependence of the steric asymmetry (see text) for CH_3Cl scattered from HOPG at 300 K in the 320 meV oriented CH_3Cl incidence. The blue dashed line corresponds to the θ_s dependence of the direct-inelastic scattering in Figure 5b.

hexapole state-selection with a beam stop. Figure 6 (top panel) also demonstrates that the molecular-orientation effect appears in the direct-inelastic scattering. The difference spectrum between the CH_3-end and the Cl-end collisions agrees well in the peak profile with the direct-inelastic component taken from Figure 4.

Figure 7 shows the θ_s dependence of the steric effect for the 320 meV oriented CH_3Cl incidence on the HOPG surface at 300 K. Here we define the steric asymmetry at each scattering angle, θ_s, as $R = (I(CH_3) - I(Cl))/(2I(\text{random}))$, where $I(CH_3)$ and $I(Cl)$ are the scattered CH_3Cl intensity at θ_s for the CH_3-end and the Cl-end collisions, respectively. As we discussed above, the steric effect appears on the direct-inelastic scattering, and thus we use the direct-inelastic component for $I(\text{random})$ of the scattered CH_3Cl intensity for the random-orientation beam. Figure 7 also shows the θ_s distribution of the direct-inelastic component with a dashed line taken from Figure 5b. The sign of R is always positive for θ_s, where the direct-inelastic

component is dominant. This result suggests that the surface-trapping probability is higher for the Cl-end collision than for the CH_3-end collision. The present outcome obtained under better-defined experimental conditions agrees well with the previous work reported by Bernstein and coworkers[20] and thus confirms the idea that in the dissociative adsorption of CH_3Cl on Si(100), the transient trapping into the shallow precursor well plays an important role on the observed steric effects.[38−40] The negative steric effect should be observed in the trapping desorption because the total flux must be conserved in the nonreactive scattering. However, as seen in Figure 5, the angular distribution is much broader for the trapping desorption so that the molecular-orientation effect in the trapping desorption becomes small enough to be undetectable in the angle-resolved measurements.

With increasing scattering angles at $\theta_s \geq 54°$, the steric effect, R, increases, suggesting that the increase in the surface-normal component of the incident energy removes the smearing of the steric effect induced by the steering effect,[40] where a CH_3Cl molecule is reoriented in the favorite direction. Here we assume that the angle-resolved measurement represents all scattering angles at a fixed angle of incidence. Another possibility may be the θ_s dependence of the energy-loss processes, which may reveal the θ_s dependence of the final kinetic energy of CH_3Cl. However, this can be ruled out because in all scattering geometry, the scattered molecules in the direct-inelastic component suffer more than 94% energy loss of the initial translational energy of 320 meV.

As we discussed above shortly, the interactions between a permanent dipole and its image dipole contribute to the scattering CH_3Cl on the HOPG surface in addition to the van der Waals dispersion interaction. It is expected that the dipole versus image-dipole attractive interaction depends strongly on the molecular orientation of an incoming molecule.[24] The Cl-end approach induces more attractive interaction than the CH_3-end approach because of the highest charge density of Cl. Therefore, the Cl-end collision suffers larger energy dissipation than the CH_3-end collision because of the acceleration near the surface. As a result, the surface trapping probability will be higher for the Cl-end collision. In a series of works by Bernstein and coworkers, the trapping probability is always higher for the side of the highest charge density.[17−24] The interaction between a permanent dipole and its image dipole may be described with a simple point-charge model. In the CF_3H scattering from the HOPG surface, such a simple approximation succeeded in explaining the observed steric effects.[24] The point-charge model is effective at a long distance from the surface,[52] whereas at the close distance around the minimum of the attractive potential well, the charge redistribution of CH_3Cl will occur and require quantum mechanical calculations. The theoretical calculations are expected for further detailed interpretation of the present experiments.

4. Summary

We report results of a study on steric effects appearing in the scattering of a CH_3Cl from HOPG surface at 300 K. The scattered CH_3Cl intensity in the CH_3-end collision is larger than that in the Cl-end collision. This steric effect appears in the direct-inelastic scattering without residence time where a CH_3Cl molecule suffers a significant energy loss. Therefore, the surface-trapping probability for the Cl-end approach is larger than that for the CH_3-end approach. These results suggest that the strong anisotropy in the interaction potential, probably due to anisotropy in the permanent-dipole versus its image-dipole interaction in a classical electromagnetic sense, induces the molecular-orientation dependence of the energy dissipation during transient trapping into the physisorption well.

Acknowledgment. We are thankful to Dr. Ellen Backus of Leiden University for her help in the initial stage of the experimental set of the TOF system. We gratefully acknowledge MEXT for a Grant-in-Aid for Scientific Research (no. 20350005). This work was also financially supported by PRESTO of JST. T.F. thanks the Global COE Program for "Global Education and Research Center for Bio-Environmental Chemistry" of Osaka University.

References and Notes

(1) Novakoski, L. V.; McClelland, G. M. *Phys. Rev. Lett.* **1987**, *59*, 1259.
(2) Jacobs, D. C.; Kolasinski, K. W.; Madix, R. J.; Zare, R. N. *J. Chem. Phys.* **1987**, *87*, 5038.
(3) Kuipers, E. W.; Tenner, M. G.; Kleyn, A. W.; Stolte, S. *Nature* **1988**, *334*, 420.
(4) Tenner, M. G.; Kuipers, E. W.; Kleyn, A. W.; Stolte, S. *J. Chem. Phys.* **1988**, *89*, 6552.
(5) Kleyn, A. W.; Kuipers, E. W.; Tenner, M. G.; Stolte, S. *J. Chem. Soc., Faraday Trans. 2* **1989**, *85*, 1337.
(6) Jacobs, D. C.; Pois, I.; Kuipers, E. W.; Kleyn, A. W.; Schröter, L.; Zacharias, D. H.; Fecher, G.; Volkmer, M.; Böwering, N.; Pawlitzky, B.; Heinzmann, U.; Levine, R. D.; Snowdon, K. J. *J. Chem. Soc., Faraday Trans. 2* **1989**, *85*, 1357.
(7) Kuipers, E. W.; Tenner, M. G.; Kleyn, A. W.; Stolte, S. *Phys. Rev. Lett.* **1989**, *62*, 2152.
(8) Tenner, M. G.; Kuipers, E.; Langhout, W. Y.; Kleyn, A. W.; Nicolasen, G.; Stolte, S. *Surf. Sci.* **1990**, *236*, 151.
(9) Geuzebroek, F. H.; Wiskerke, A. E.; Tenner, M. G.; Kleyn, A. W.; Stolte, S.; Namiki, A. *J. Phys. Chem.* **1991**, *95*, 8409.
(10) Tenner, M. G.; Kuipers, E. W.; Kleyn, A. W.; Stolte, S. *Surf. Sci.* **1991**, *242*, 376.
(11) Heinzmann, U.; Holloway, S.; Kleyn, A. W.; Palmer, R. E.; Snowdon, K. J. *J. Phys.: Condens. Matter* **1996**, *8*, 3254.
(12) Lahaye, R. J. W. E.; Stolte, S.; Holloway, S.; Kleyn, A. W. *J. Chem. Phys.* **1996**, *104*, 8301.
(13) Kleyn, A. W. *Prog. Surf. Sci.* **1997**, *54*, 304.
(14) Komorowski, A. J.; Ternow, H.; Razaznejad, R.; Berenbak, B.; Sexton, J. Z.; Zoric, I.; Kasemo, B.; Lundqvist, B. I.; Stolte, S.; Kleyn, A. W.; Kummel, A. C. *J. Chem. Phys.* **2002**, *117*, 8185.
(15) Berenbak, B.; Riedmüller, B.; Stolte, S.; Kleyn, A. W. *Chem. Phys.* **2004**, *301*, 309.
(16) Sitz, G. O. *Rep. Prog. Phys.* **2002**, *65*, 1165.
(17) Curtiss, T. J.; Bernstein, R. B. *Chem. Phys. Lett.* **1989**, *161*, 212.
(18) Mackay, R. S.; Curtiss, T. J.; Bernstein, R. B. *Chem. Phys. Lett.* **1989**, *164*, 341.
(19) Mackay, R. S.; Curtiss, T. J.; Bernstein, R. B. *J. Chem. Phys.* **1990**, *92*, 801.
(20) Curtiss, T. J.; Mackay, R. S.; Bernstein, R. B. *J. Chem. Phys.* **1990**, *93*, 7387.
(21) Ionov, S. I.; Lavilla, M. E.; Mackay, R. S.; Bernstein, R. B. *J. Chem. Phys.* **1990**, *93*, 7406.
(22) Ionov, S. I.; Lavilla, M. E.; Bernstein, R. B. *J. Chem. Phys.* **1990**, *93*, 7416.
(23) Ionov, S. I.; Bernstein, R. B. *J. Chem. Phys.* **1991**, *94*, 1564.
(24) Ionova, S. V.; Ionov, S. I.; Bernstein, R. B. *J. Phys. Chem.* **1991**, *95*, 8371.
(25) Whitehouse, D. B.; Buckingham, A. D.; Bernstein, R. B.; Cho, V. A.; Levine, R. D. *J. Phys. Chem.* **1991**, *95*, 8175.
(26) Fecher, G. H.; Böwering, N.; Volkmer, M.; Pawlitzky, B.; Heinzmann, U. *Surf. Sci.* **1990**, *230*, L169.
(27) Müller, H.; Dierks, B.; Hamza, F.; Zagatta, G.; Fecher, G. H.; Böwering, N.; Heinzmann, U. *Surf. Sci.* **1992**, *269/270*, 207.
(28) Müller, H.; Zagatta, G.; Brandt, M.; Wehmeyer, O.; Böwering, N.; Heinzmann, U. *Surf. Sci.* **1994**, *307/309*, 159.
(29) Brandt, M.; Müller, H.; Zagatta, G.; Wehmeyer, O.; Böwering, N.; Heinzmann, U. *Surf. Sci.* **1995**, *331/333*, 30.
(30) Brandt, M.; Müller, H.; Zagatta, G.; Böwering, N.; Heinzmann, U. *Surf. Sci.* **1996**, *352/354*, 290.
(31) Brandt, M.; Zagatta, G.; Böwering, N.; Heinzmann, U. *Surf. Sci.* **1997**, *385*, 346.
(32) Brandt, M.; Gerber, T.; Böwering, N.; Heinzmann, U. *Phys. Rev. Lett.* **1998**, *81*, 2376.
(33) Brandt, M.; Gerber, T.; Kuhlmann, F.; Böwering, N.; Heinzmann, U. *Surf. Sci.* **1998**, *402/404*, 160.

(34) Brandt, M.; Kuhlmann, F.; Gerber, T.; Böwering, N.; Heinzmann, U. *Surf. Sci.* **1999**, *439*, 49.

(35) Hou, H.; Gulding, S. J.; Rettner, C. T.; Wodtke, A. M.; Auerbach, D. J. *Science* **1997**, *277*, 80.

(36) Vattuone, L.; Gerbi, A.; Rocca, M.; Valbusa, U.; Pirani, F.; Vecchiocattivi, F.; Cappelletti, D. *Angew. Chem., Int. Ed.* **2004**, *43*, 5200.

(37) Gerbi, A.; Savio, L.; Vattuone, L.; Pirani, F.; Cappelletti, D.; Rocca, M. *Angew. Chem., Int. Ed.* **2006**, *45*, 6655.

(38) Okada, M.; Goto, S.; Kasai, T. *Phys. Rev. Lett.* **2005**, *95*, 176103.

(39) Okada, M.; Goto, S.; Kasai, T. *J. Am. Chem. Soc.* **2007**, *129*, 10052.

(40) Okada, M.; Goto, S.; Kasai, T. *J. Phys. Chem. C* **2008**, *112*, 19612.

(41) Hashinokuchi, M.; Okada, M.; Ito, H.; Kasai, T.; Moritani, K.; Teraoka, Y. *Phys. Rev. Lett.* **2008**, *100*, 256104.

(42) Okada, M.; Moritani, K.; Goto, S.; Kasai, T. *Jpn. J. Appl. Phys.* **2005**, *44*, 8580.

(43) The background of the TOF spectrum for the CH_3Cl(5%) seeded in Ne is small enough for the determination of the exact beam profile. Therefore, we measured the beam profile of the CH_3Cl(5%) seeded in Ne and He with varying rare-gas ratio and crosschecked the beam profile for the CH_3Cl(5%) seeded in He.

(44) Bulthuis, J.; Milan, J. B.; Janssen, M. H. M.; Stolte, S. *J. Chem. Phys.* **1991**, *94*, 7181.

(45) Sasaki, M.; Yoshida, S. *Surf. Sci.* **1994**, *315*, L964.

(46) Sasaki, M.; Yoshida, S. *Jpn. J. Appl. Phys.* **1994**, *33*, L884.

(47) In the present experiments, we used the pulsed-valve generated beam as it is. Therefore, the pulse width is not short enough to determine the surface residence time. Here the upper limit of the surface residence time is presented.

(48) Watanabe, Y.; Yamaguchi, H.; Hashinokuchi, M.; Sawada, K.; Maruyama, S.; Matsumoto, Y.; Shobatake, K. *Eur. Phys. J. D* **2006**, *38*, 103.

(49) Watanabe, Y.; Yamaguchi, H.; Hashinokuchi, M.; Sawada, K.; Maruyama, S.; Matsumoto, Y.; Shobatake, K. *Chem. Phys. Lett.* **2005**, *413*, 331.

(50) Kondo, T.; Mori, D.; Okada, R.; Sasaki, M.; Yamamoto, S. *J. Chem. Phys.* **2005**, *123*, 114712.

(51) Townes, C. H.; Schawlow, A. L. *Microwave Spectroscopy*; McGraw-Hill: New York, 1955.

(52) Fernández-Torre, D.; Kupiainen, O.; Pyykkö, P.; Halonen, L. *Chem. Phys. Lett.* **2009**, *471*, 239.

JP904893Z